Journal of Solid State Chemistry 182 (2009) 2030–2035

Contents lists available at ScienceDirect

Journal of Solid State Chemistry

journal homepage: www.elsevier.com/locate/jssc

Phase transition behavior for $ZrW_{2-x}Mo_xO_8$ compositions at elevated temperatures

Yongfang Shi [a,b], Xi Chen [a], Jingsa Han [a], Hui Ma [a], Xiaoxia Li [a], Xiaojing Yang [a], Xinhua Zhao [a,*]

[a] College of Chemistry and Analysis and Test Center, Beijing Normal University, Beijing 100875, PR China
[b] Fujian Institute of Research on the Structure of Matter, Chinese Academy of Sciences, Fuzhou, Fujian 350002, PR China

ARTICLE INFO

Article history:
Received 31 December 2008
Received in revised form
21 April 2009
Accepted 7 May 2009
Available online 22 May 2009

Keywords:
Materials science
Phase diagrams
Phase transformation
Negative thermal expansion
ZrW_2O_8

ABSTRACT

A systematical study on cubic $ZrW_{2-x}Mo_xO_8$ ($x = 0.73, 0.53, 0.33, 0.11$) solid solutions reveals that their temperature-dependent phase transition behaviors are related to the Mo fraction x. A phase diagram of cubic $ZrW_{2-x}Mo_xO_8$ solid solutions has been drawn over a wide temperature range (298–1473 K) on the basis of the temperature-dependent phase transition behaviors observed.

1. Introduction

Negative thermal expansion (NTE) materials are widely used for controlling the effective thermal expansion coefficient of composites. Special attention has been paid to cubic ZrW_2O_8 (c-ZrW_2O_8) and cubic $ZrMo_2O_8$ (γ-$ZrMo_2O_8$) compounds due to their isotropic NTE property over a wide temperature range (0.5–1050 K for c-ZrW_2O_8 and 11–573 K for γ-$ZrMo_2O_8$) [1–3]. However, the order–disorder phase transformation around 433 K for c-ZrW_2O_8 leads to a remarkable deviation from the linear temperature-dependence of expansion coefficient from -8.8×10^{-6} to $-4.9\times10^{-6}\,K^{-1}$. Moreover an irreversible phase transformation was observed for orthorhombic structure (γ-ZrW_2O_8) under pressure of 0.21 GPa at ambient room temperature [4,5]. These phase transformations make c-ZrW_2O_8 difficult to be commercially used as a kind of practical NTE filler of composites. The defects might be improved by fusing it together with γ-$ZrMo_2O_8$, because the latter remarkably reduces its phase transition temperature and increase its compression resistance (0.7 GPa) [3,6]. Unfortunately, γ-$ZrMo_2O_8$ appears to be metastable, and furthermore, the synthesis process, through dehydration of its corresponding precursor prepared in acidic solution, could be complicated because a series of factors affect the preparation of the precursor and the dehydration can be accomplished only within a very narrow temperature range [7,8]. Some successful attempts have been reported to improve the compression resistance as well as depress the phase transformation temperature of c-ZrW_2O_8 by synthesizing $ZrW_{2-x}Mo_xO_8$ solid solutions [9–12]. The phase behavior of the pseudobinary ZrW_2O_8–$ZrMo_2O_8$ system demonstrates that below 1073 K the $ZrW_{2-x}Mo_xO_8$ solid solutions can stabilize the cubic structure within a wide composition range [13].

In this paper a series of cubic $ZrW_{2-x}Mo_xO_8$ ($x = 0.73$, 0.53, 0.33, 0.11) solid solutions are synthesized. We first investigate their phase transition behaviors from room temperature up to 1473 K by using X-ray diffraction (XRD) phase analysis, differential scanning calorimetric (DSC), thermal gravimetric (TG) techniques and mass loss analysis. The obtained phase diagram indicates that their phase transformation behaviors are different from each other, depending on the composition x and temperature.

2. Experimental

Cubic $ZrW_{2-x}Mo_xO_8$ (denoted as c-$ZrW_{2-x}Mo_xO_8$, $x = 0.73$, 0.53, 0.33, 0.11) solid solutions were synthesized by mixing commercially available reagents $ZrOCl_2\cdot8H_2O$, $(NH_4)_6Mo_7O_{24}\cdot4H_2O$ and $5(NH_4)_2O\cdot12WO_3\cdot5H_2O$ in aqueous solution with atomic ratios 1:1.2:0.8, 1:1.4:0.6, 1:1.6:0.4, and 1:1.8:0.2 of Zr:W:Mo according to the method described previously [14]. The mixtures was heated up to 873 K in 4 h [14], producing trigonal solid solutions of $ZrW_{2-x}Mo_xO_8$ ($x = 0.8, 0.6, 0.4$) together with an amorphous precursor $ZrO_2\cdot1.8WO_3\cdot0.2MoO_3\cdot$ (the XRD patterns

* Corresponding author. Fax: +86 010 58802075.
E-mail address: xinhuaz@bnu.edu.cn (X. Zhao).

0022-4596/$ - see front matter © 2009 Elsevier Inc. All rights reserved.
doi:10.1016/j.jssc.2009.05.017

are deposited in Fig.S1 of supporting information), and further heating 1 h at different temperatures (as listed in Table 1) yields the initial c-$ZrW_{2-x}Mo_xO_8$. The mass loss during annealing the trigonal and amorphous precursors was monitored by weighing the c-$ZrW_{2-x}Mo_xO_8$ samples quenched at ambient atmosphere. The sublimates were dissolved in basic solution and determined quantitatively with inductively coupled plasma-atomic emission spectrometry (ICP-AES, JY, ULTIMA). The results indicate that the sublimates in the procedures basically consisted of MoO_3 (trace WO_3 was ignored) for c-$ZrW_{2-x}Mo_xO_8$ preparation. Therefore the accurate compositions of the initial c-$ZrW_{2-x}Mo_xO_8$ solid solutions are departure from the atomic ratios of the batch and were re-deduced as listed in Table 1.

The phase behaviors of the c-$ZrW_{2-x}Mo_xO_8$ ($x = 0.73$, 0.53, 0.33, 0.11) solid solutions were investigated by *in-situ* variable temperature XRD from the room temperature to 1173 K and *ex-situ* XRD at the room temperature. The cylindrical pellets of cubic solid solution samples which were pressed under 4 MPa for about 0.6 g powders were prepared by annealing the samples at designed temperatures for *ex-situ* XRD measurements as listed in Table 2. The pellet samples $ZrW_{2-x}Mo_xO_8$ ($x = 0.73$, 0.53, 0.33, 0.11) were retained at each assigned temperature (Table 2) for 30 min (hereafter denoted as annealed-samples). The annealing temperatures were selected according to DSC and TG data.

The DSC curves were recorded at heating rate of 25 K min^{-1} using a DTA-404 PC (Netzsch) under air–atmosphere within temperature range of 873–1473 K, and an empty Pt crucible was used as the reference. TG curves were measured for about 0.01 g powder of each initial c-$ZrW_{2-x}Mo_xO_8$ sample with TG-DTA (ZRP-2P, Shanghai, China) instrument. The mass of annealed-sample $ZrW_{2-x}Mo_xO_8$ was weighed after annealing at different temperatures and the composition changes were deduced from the mass loss which was determined to be the sublimate of MoO_3.

The Powder XRD data were collected on Philips X-Pert MPD diffractometer with X'Celerator detector using Cu$K\alpha$ radiation (40 kV, 40 mA). *Ex-situ* XRD data at the room temperature from 10° to 70° (2θ) and *in-situ* variable temperature XRD data from 10° to 80° (2θ) were collected in 5 min with a step width of 0.0167° (2θ) and step-time of 10 s under the ambient atmosphere. Each ground sample was mounted on a platinum strip, which served as sample holder as well as heater attached with Anton Parr high-temperature units used for *in-situ* variable temperature XRD measurements. The *in-situ* variable temperature XRD data of the c-$ZrW_{2-x}Mo_xO_8$ samples annealed for 3 min at every temperature were collected at a temperature ramp of 10 K min^{-1} within the temperature range of 298–1073 K. The sample temperatures were calibrated with KCl as external standard using the experimental relationship between lattice parameter a_t and temperature t, [15] in which the standard KCl was mixed with ZrW_2O_8 to correct the big thermal hysteresis between them (the calibration process is described in S1 and Fig.S2 of Supporting Information).

The XRD patterns of $ZrW_{2-x}Mo_xO_8$ phases were indexed using the PowderX software suite, [16] and the accurate lattice parameters were deduced using Unitcell program [17] from the XRD data calibrated with SiO_2 as the internal standard (PDF #33–1161). The quantitative crystal phase analysis of annealed-sample $ZrW_{1.47}Mo_{0.53}O_8$, which is related to the annealing temperature, is conducted with Rietveld refinement by using GSAS software [18,19]. The structure models of the cubic and trigonal $ZrW_{1.47}Mo_{0.53}O_8$ phases, [2,20] and WO_3 (ICSD #16080) and ZrO_2 (ICSD #94887) oxides are referred to the literatures in the structure refinements.

Table 1
The synthetic temperature and composition of cubic $ZrW_{2-x}Mo_xO_8$.

Composition		Weight loss (wt%)	Synthetic temperature (K)
Precursor	Cubic phase $ZrW_{2-x}Mo_xO_8$[a]		
$ZrW_{1.2}Mo_{0.8}O_8$	$ZrW_{1.27}Mo_{0.73}O_8$	2.6	1273
$ZrW_{1.4}Mo_{0.6}O_8$	$ZrW_{1.47}Mo_{0.53}O_8$	2.1	1323
$ZrW_{1.6}Mo_{0.4}O_8$	$ZrW_{1.67}Mo_{0.33}O_8$	2.0	1373
$ZrW_{1.8}Mo_{0.2}O_8$	$ZrW_{1.89}Mo_{0.11}O_8$	2.0	1423

[a] Calculated according to MoO_3 loss during synthesis.

3. Results and discussion

3.1. Characteristics of cubic $ZrW_{2-x}Mo_xO_8$ ($x = 0.73$, 0.53, 0.33, 0.11)

The XRD patterns of the initial $ZrW_{2-x}Mo_xO_8$ ($x = 0.73$, 0.53, 0.33, 0.11) solid solutions were indexed to cubic structure of α-ZrW_2O_8 with the space group $P2_13$ [1] after heating at synthetic temperature in Table 1. Fig. 1 is the XRD pattern of cubic $ZrW_{1.27}Mo_{0.73}O_8$ in addition of trace reflections of ZrO_2, as an example of these solid solutions. (The XRD patterns of others are deposited in Figs. S3, S4, S5 of Supporting Information.) As shown, it is well-crystallized without detectable amorphous broad band. Therefore, the compositions of initial c-$ZrW_{2-x}Mo_xO_8$ ($x = 0.73$, 0.53, 0.33,

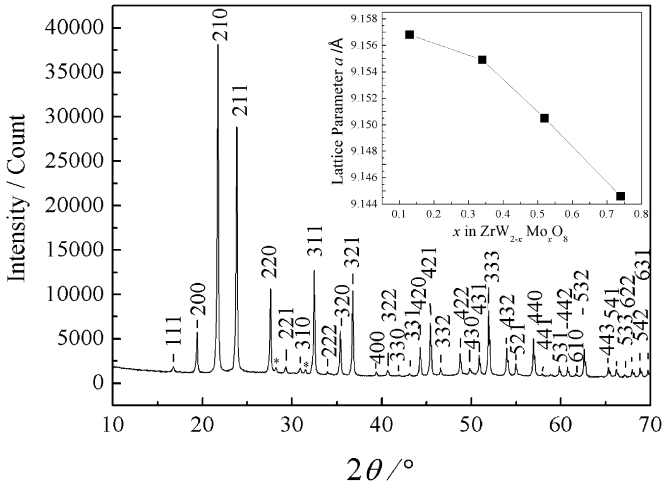

Fig. 1. The indexed X-ray diffraction pattern for c-$ZrW_{1.27}Mo_{0.73}O_8$ and the lattice parameters of c-$ZrW_{2-x}Mo_xO_8$ ($x = 0.73$, 0.53, 0.33, 0.11) in the inset. The asterisks represent the trace reflections of ZrO_2.

Table 2
The annealing temperature for annealed-samples of cubic $ZrW_{2-x}Mo_xO_8$.

The initial composition	Annealing temperature (K)										
$ZrW_{1.27}Mo_{0.73}O_8$	913	933	1023	1073	1123	1163	1173	1183	1193	1273	1323
$ZrW_{1.47}Mo_{0.53}O_8$	923	973	1073	1123	1173	1193	1223	1253	1273	1323	1373
$ZrW_{1.67}Mo_{0.33}O_8$	973	1073	1123	1173	1223	1273	1323	1373	1423		
$ZrW_{1.89}Mo_{0.11}O_8$	923	973	1073	1173	1273	1323	1373	1383	1393	1423	1453

0.11) solid solutions were determined precisely as listed in Table 1, by taking into account of mass loss due to MoO_3 sublimation during annealing at synthetic temperature. The lattice parameters *a*'s of the series samples decrease with increasing Mo-fraction *x*.

3.2. XRD and DSC–TG analysis of c-$ZrW_{2-x}Mo_xO_8$ ($x = 0.73, 0.53, 0.33, 0.11$)

The phase behaviors were studied by the XRD *in-situ* measurement from the room temperature to 1073 K using the powder samples of initial c-$ZrW_{2-x}Mo_xO_8$ and by *ex-situ* measurement for higher temperatures using the annealed-samples of $ZrW_{2-x}Mo_xO_8$.

Analysis of *in-situ* XRD patterns of c-$ZrW_{2-x}Mo_xO_8$ solid solutions ($x = 0.73$, 0.53) shown in Fig. 2 reveals that the phase transformation occurs from cubic to trigonal phase. These solid solutions $ZrW_{1.27}Mo_{0.73}O_8$ and $ZrW_{1.47}Mo_{0.53}O_8$ formed at high temperature have a trigonal crystal structure with $a = 5.8362(1)$ and $c = 6.0694(4)$ Å, and $a = 5.8439(7)$ and $c = 6.0727(9)$ Å, respectively, similar to that of HTT-$ZrWMoO_8$ ($a = 5.8404(1)$ and $c = 6.0671(2)$ Å) [20]. Fig. 3 shows DSC curves of the c-$ZrW_{2-x}Mo_xO_8$ samples, which are smooth exothermic ones without sharp peaks until the temperature increase up to 1173 K, showing the phase transformation is a continuous process from metastable cubic to stable trigonal phase. Therefore, the phase-transformation temperatures can be obtained precisely from XRD patterns, being 861 and 889 K for c-$ZrW_{2-x}Mo_xO_8$ solid solutions of $x = 0.73$ and 0.53, respectively.

For *ex-situ* XRD measurement of annealed-samples $ZrW_{2-x}Mo_xO_8$ ($x = 0.73$ and 0.53), the XRD patterns (Fig. 4) indicate that the samples transform from a metastable cubic to stable trigonal phase at higher temperatures than those of the *in-situ* variable temperature measurements for powder samples.

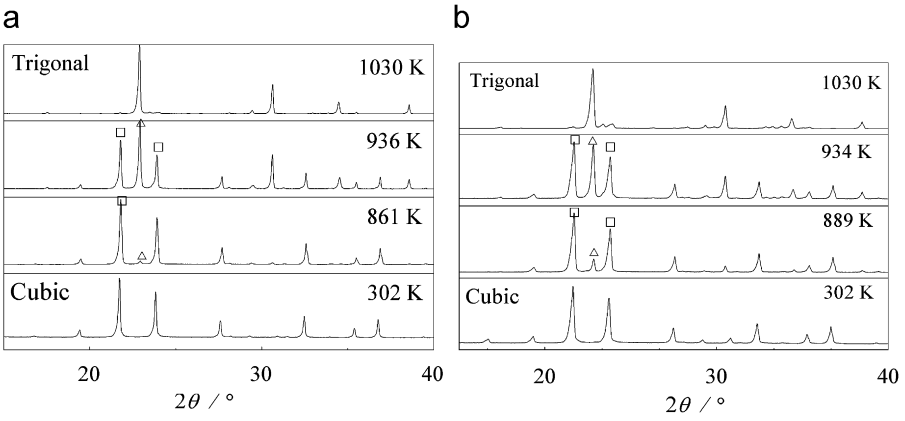

Fig. 2. The *in-situ* variable temperature XRD patterns of initial c-$ZrW_{2-x}Mo_xO_8$ at different temperatures: (a) $x = 0.73$; (b) $x = 0.53$. The reflection marks denote polymorphs: (△): trigonal; (□): cubic.

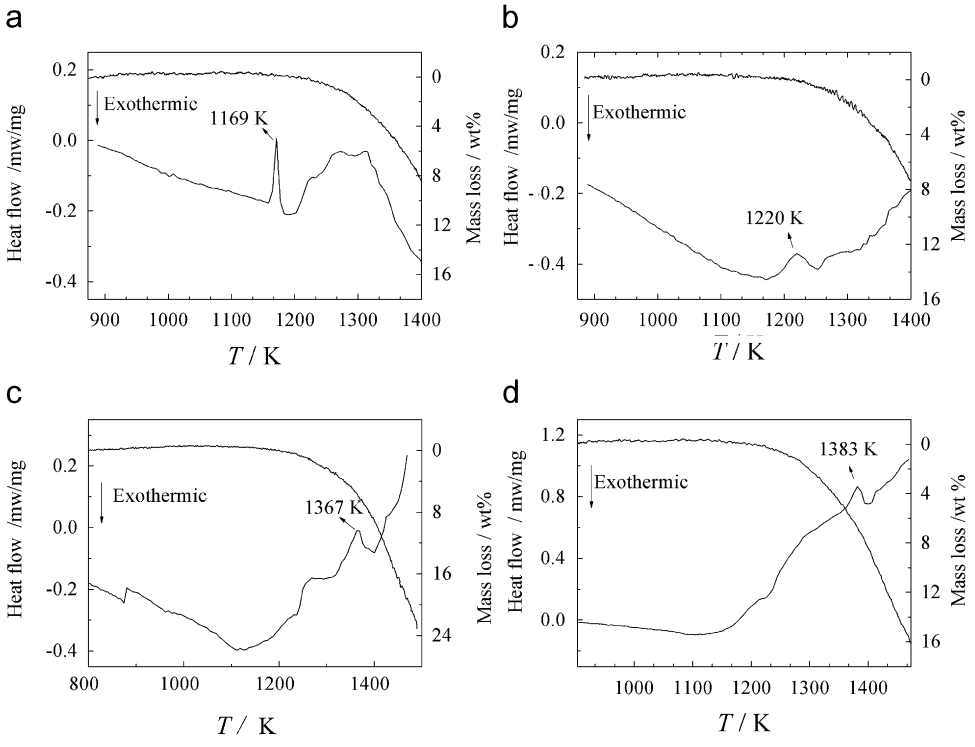

Fig. 3. DSC–TG curves for initial c-$ZrW_{2-x}Mo_xO_8$, (a) $x = 0.73$, (b) $x = 0.53$, (c) $x = 0.33$, and (d) $x = 0.11$.

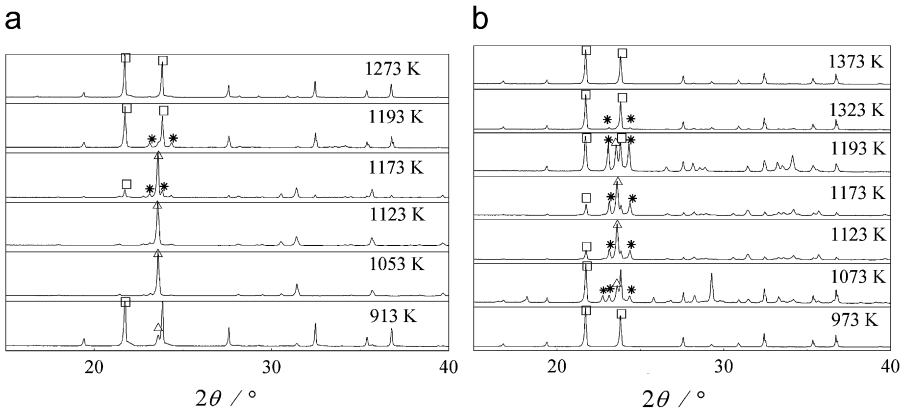

Fig. 4. The *ex-situ* XRD patterns of annealed-samples at room temperatures: (a) $x = 0.73$; (b) $x = 0.53$. The reflection marks denote polymorphs: (△): trigonal; (□): cubic; and (∗): WO_3.

Typically comparing Fig. 4 with Fig. 2, 913 vs. 861 K the trigonal reflection appears for $ZrW_{1.27}Mo_{0.73}O_8$ but the transformation did not occur for annealed-sample $ZrW_{1.47}Mo_{0.53}O_8$ at 973 K which is above the phase transformation temperature 889 K in Fig. 2. The increasing of the phase transition temperature may be related to the increase of the stress during the phase transition process of sample preparation for *ex-situ* measurements.

The *ex-situ* XRD pattern of $ZrW_{1.27}Mo_{0.73}O_8$ reveals that the trigonal phase is stable in the temperature range from 1053 to 1123 K, but a cubic phase appears at 1173 K. Such trigonal-to-cubic phase transformation is consistent with the result of an endothermic peak at 1169 K in the DSC curve. At the same time, the cubic phase may be able to decompose slightly on the surface of the pellet, as indicated by the occurrence of a very weak reflection of WO_3 accompanied by a small mass loss of MoO_3 (less than 0.5 wt%) at 1173 K. Of interest is that the reflection intensity of WO_3 does not change upon extending the sintering duration and increasing temperature within a narrow "temperature window" ranged from 1173 to 1193 K. This suggests that the decomposition of $ZrW_{1.27}Mo_{0.73}O_8$ solid solution turns out to be localized on the sample surface rather than penetrated into the whole sample body. The color change from white to pale-yellow observed only on the sample surface provides additional evidence. However, above 1193 K, the reflection of WO_3 decreases accompanied with an enhancement of cubic phase reflections. It suggests that WO_3 is capable of reacting with $ZrW_{1.27}Mo_{0.73}O_8$ solid solution itself, leading to the formation of a new cubic solid solution with enriched W-fraction, and the residual ZrO_2 remains in the sample.

On the contrary, the XRD (Fig. 4b) for the annealed-sample $ZrW_{1.47}Mo_{0.53}O_8$ indicates the reflections of WO_3 appear together with the cubic-to-trigonal phase transformation within the temperature range from 1073 to 1193 K. That is, the annealed-sample of the pellet $ZrW_{1.47}Mo_{0.53}O_8$ solid solution exists as a mixture consisted of its trigonal and cubic phase together with a trace of WO_3 and ZrO_2 produced by the decomposition. Comparing with the annealed-sample of $ZrW_{1.27}Mo_{0.73}O_8$ the narrow "temperature window" characteristic of pure trigonal phase is not shown in $ZrW_{1.47}Mo_{0.53}O_8$ solid solution.

The temperature-dependence of the mass fraction related to the transformation between different crystal phases for $ZrW_{1.47}Mo_{0.53}O_8$ system is displayed in Fig. 5. It is clear that the decrease of the cubic phase in the solid solution with temperature increasing implies that transformation from metastable c-$ZrW_{1.47}Mo_{0.53}O_8$ to trigonal phase occurs together with partial decomposition, which leads to formation of WO_3 and ZrO_2, within a range of 973–1123 K. Within the temperature range of 1123–1173 K, the

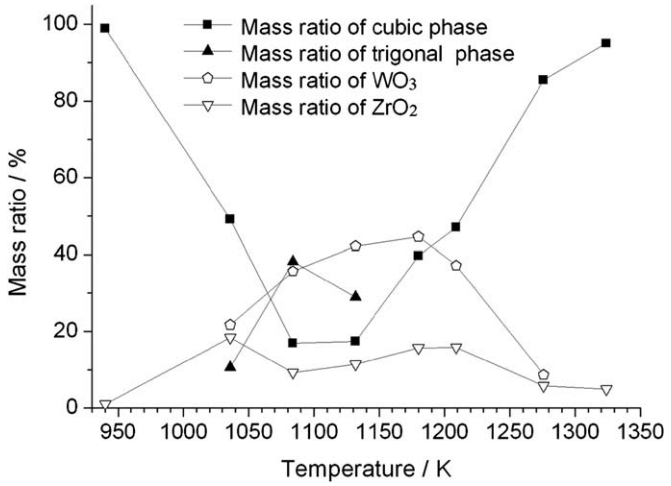

Fig. 5. The mass fraction of different crystal phases plotted against the temperature for $ZrW_{1.47}Mo_{0.53}O_8$ annealed-samples.

cubic phase is invariable, but trigonal phase decreases slowly with temperature increasing. This result suggests that the transformation from cubic to trigonal is almost completed at 1123 K, above the temperature the trigonal phase slowly decomposes to component oxides; whereas the oxides do not react with $ZrW_{1.47}Mo_{0.53}O_8$ to form W-rich $ZrW_{2-x}Mo_xO_8$ solid solution between 1123 and 1173 K.

Above 1220 K, the fast increase of the cubic phase compared with the disappearance of trigonal phase indicates that trigonal phase transformation of $ZrW_{1.47}Mo_{0.53}O_8$ to cubic phase occurs at a high rate while remained WO_3 and ZrO_2 reacted with $ZrW_{1.48}Mo_{0.52}O_8$ to form W-rich cubic $ZrW_{2-x}Mo_xO_8$ solid solution. Hence the endothermic peak in the DSC curve of $ZrW_{1.47}Mo_{0.53}O_8$ (Fig. 3b) can be attributed to the reaction temperature of the trigonal phase $ZrW_{1.48}Mo_{0.52}O_8$ with component oxides (WO_3 and ZrO_2) to form W-rich cubic $ZrW_{2-x}Mo_xO_8$ at 1220 K. It is consistent with the XRD pattern in Fig. 4b, which also indicates the complete conversion of $ZrW_{2-x}Mo_xO_8$ from trigonal and oxide phases to W-rich cubic phase at 1373 K.

The phase behavior of c-$ZrW_{2-x}Mo_xO_8$ ($x = 0.33$ and 0.11) solid solutions are similar to each other, i.e., they decompose to component oxides instead of changing to trigonal phase at high temperature (Fig. 6). The decomposition temperature of c-$ZrW_{2-x}Mo_xO_8$ ($x = 0.33$, 0.11) are 917 K for powder samples and 1073 K for annealed-samples, respectively. In Fig. 6b, it is noticeable that

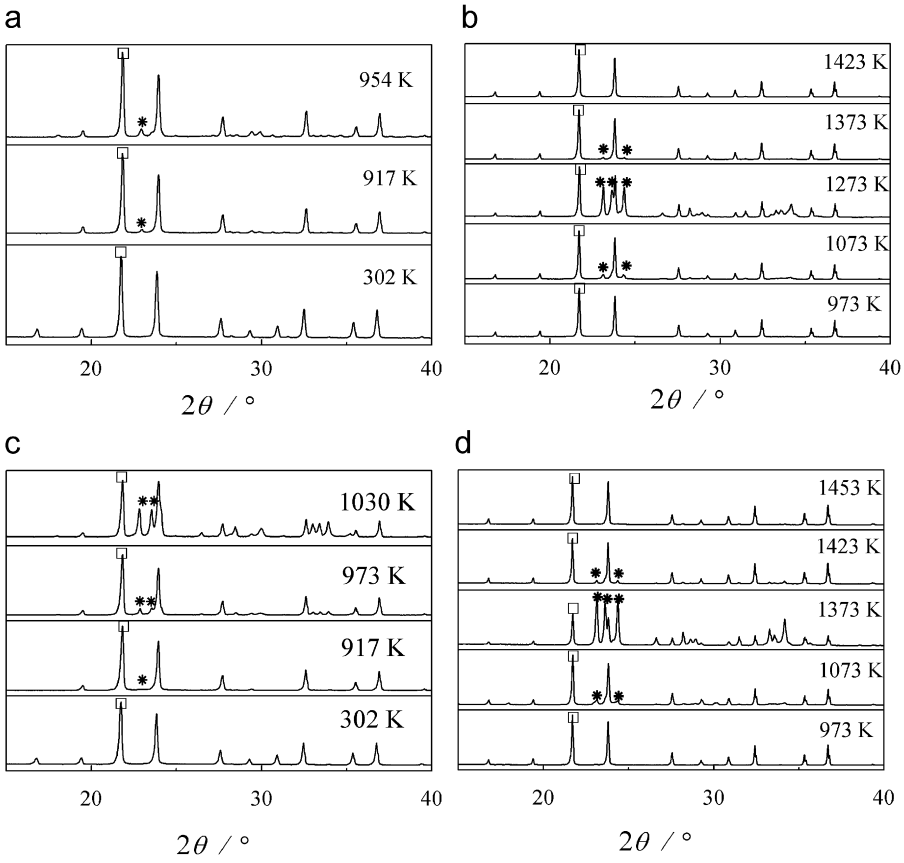

Fig. 6. The *in-situ* variable temperature XRD patterns of initial c-$ZrW_{2-x}Mo_xO_8$ at different temperatures (a, c) and *ex-situ* XRD patterns of annealed-samples $ZrW_{2-x}Mo_xO_8$ (b, d) at room temperature (a, b: $x = 0.33$ and c, d: $x = 0.11$), respectively. The reflection marks denotation: (□): cubic; (∗): WO_3.

the peak intensities of the oxides decrease markedly inversely with that of cubic phase of $ZrW_{1.67}Mo_{0.33}O_8$ from 1273 to 1373 K, so the endothermic peak at 1367 K in the DSC curve of $ZrW_{1.67}Mo_{0.33}O_8$ (Fig. 2c) can most likely be assigned to the reaction temperature of cubic $ZrW_{1.67}Mo_{0.33}O_8$ with the remained oxides that leads the formation of W-rich cubic $ZrW_{2-x}Mo_xO_8$ solid solution. Resembling to $ZrW_{1.67}Mo_{0.33}O_8$, it is reasonable to accept that the similar reaction of the cubic $ZrW_{1.89}Mo_{0.11}O_8$ with the remained oxides occurs between 1373 and 1423 K. For this reason, the endothermic peak of the DSC curve at 1383 K in Fig. 2d can be assigned to thermal effect of the reaction of cubic $ZrW_{1.89}Mo_{0.11}O_8$ with the oxides leading to W-rich cubic $ZrW_{2-x}Mo_xO_8$ formation. The composition of the W-enriched $ZrW_{2-x}Mo_xO_8$ solid solution is calculated by the mass loss of the annealed-sample.

The mass loss of annealed-sample $ZrW_{2-x}Mo_xO_8$ increases linearly with an increase of temperature in the region above 1173 K (Fig. 7). Although the amount of weight loss is less for annealed-sample at each temperature than that of TG curves (Fig. 3) indicated during continuous increasing temperature process, the trend is similar each other above 1173 K (the data are listed in Table S1 in Supporting Information).

The similar temperature-dependences of mass losses are observed for $ZrW_{2-x}Mo_xO_8$ solid solutions with $x = 0.53$, 0.33 and 0.11, implying that the three samples suffer a thermal decomposition together with MoO_3 sublimation. The departure of the mass loss of $ZrW_{1.89}Mo_{0.11}O_8$ from linear relationship above 1373 K indicates that the sublimation process is interrupted in the higher temperature region, where almost all MoO_3 is sublimated out but cubic ZrW_2O_8 is introduced with a trace of ZrO_2 as the residue. Compared with mass loss of $ZrW_{2-x}Mo_xO_8$ ($x = 0.53$, 0.33 and 0.11) a fast decomposition and sublimation occurs for $ZrW_{1.27}Mo_{0.73}O_8$ solid solution.

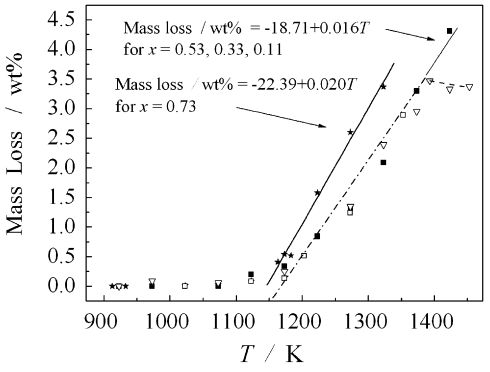

Fig. 7. The mass loss fraction dependence on the temperature for $ZrW_{2-x}Mo_xO_8$ ($x = 0.73$ ★, 0.53 □, 0.33 ■, 0.11 ▽▼) annealed-samples.

Based on the phase behavior depending on the temperature, accompanying with the sublimation discussed above, it can be deduced that a small portion of cubic solid solution decomposes and above the composition-dependent reaction temperature, the W-rich solid solution is suggested to be formed following reaction Eq. (1):

$$ZrW_{2-x}Mo_xO_8\ (s) = ZrW_{(4-2x)/(2-xy)}Mo_{2x(1-y)/(2-xy)}O_8\ (s) + (xy/2)\ ZrO_2\ (s) + xyMoO_3\ (g) \quad (1)$$

The amount of the sublimation during the heating can be calculated according to the linear function of mass loss ratio against temperature as displayed in Fig. 7. Therefore, according to

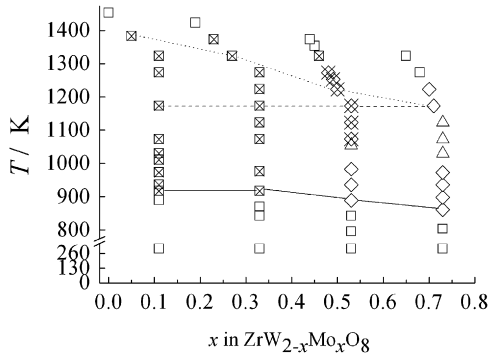

Fig. 8. The phase behavior–temperature relationship of $ZrW_{2-x}Mo_xO_8$ system. The phase denoted with symbol: (□): cubic; (△): trigonal; (×): oxides; (◇): cubic and trigonal; (⊠): cubic and oxides; (⊗): cubic, trigonal and oxides. The temperature threshold of phase transition: (—); metastable cubic transition; (- - - - - - -): MoO_3 sublimation; (▪▪▪▪▪): reaction to form W-rich $ZrW_{2-x}Mo_xO_8$.

the Eq. (1), the compositions of the W-rich solid solutions $ZrW_{2-x}Mo_xO_8$ could be evaluated from the sublimates.

3.3. *Phase transition behaviors of cubic $ZrW_{2-x}Mo_xO_8$*

The temperature-dependence phase transition behavior is constructed in Fig. 8 based on the phase behavior of powder sample below 1073 K and that of annealed-sample above 1073 K for c-$ZrW_{2-x}Mo_xO_8$ ($x = 0.73$, 0.53, 0.33, 0.11), respectively. The DSC peak temperature is adopted as the threshold of phase transition. In some cases the phase transition temperature obtained by appearance of a phase reflection from *in-situ* XRD measurement.

The metastable cubic phases of $ZrW_{2-x}Mo_xO_8$ are dynamically stable below 861 K and can be, at high temperature, either transformed to trigonal phase when $x = 0.73$, 0.53 or decomposed to component oxides (WO_3 and ZrO_2) when $x = 0.33$, 0.11. The corresponding transformation temperatures decrease with an increase of the Mo concentration for $x = 0.73$, 0.53 but decomposition temperatures are invariable with the Mo concentration for $x = 0.33$, 0.11. Trigonal polymorph is more stable companying with Mo concentration increasing, resulting in no decomposition occurring in $x = 0.73$. On the other side, no trigonal polymorph was detected for $x = 0.33$ and 0.11. The temperature of 1173 K is a constant one at which sublimation takes place together with a partial decomposition of $ZrW_{2-x}Mo_xO_8$, forming component oxides (WO_3 and ZrO_2). Above the composition-dependent reaction temperature, the stable W-rich cubic phase $ZrW_{2-x}Mo_xO_8$ recovered by the reaction. As shown in Fig. 8, the compositions of the recovered c-$ZrW_{2-x}Mo_xO_8$ are shifted towards W-rich side.

Acknowledgments

The supports by Project 20471010 of National Natural Science Foundation of China and the Foundation of Beijing Key Discipline of Inorganic Chemistry of Beijing Education Committee are gratefully acknowledged.

Appendix A. Supplementary material

Supplementary data associated with this article can be found in the online version at doi:10.1016/j.jssc.2009.05.017.

References

[1] T.A. Mary, J.S.O. Evans, T. Vogt, A.W. Sleight, Science 272 (1996) 90.
[2] J.S.O. Evans, T.A. Mary, T. Vogt, M.A. Subramanian, A.W. Sleight, Chem. Mater. 8 (1996) 2809.
[3] C. Lind, A.P. Wilkinson, Z. Hu, S. Short, J.D. Jorgensen, Chem. Mater. 10 (1998) 2335.
[4] J.S.O. Evans, Z. Hu, J.D. Jorgensen, D.N. Argyriou, S. Short, A.W. Sleight, Science 275 (1997) 61.
[5] Z. Hu, J.D. Jorgensen, S. Teslic, S. Short, D.N. Argyriou, J.S.O. Evans, A.W. Sleight, Phys. B 241 (1998) 370.
[6] C. Lind, D.G. VanDerveer, A.P. Wilkinson, J. Chen, M.T. Vaughan, D.J. Weidner, Chem. Mater. 13 (2001) 487.
[7] C. Lind, A.P. Wilkinson, C.J. Rawn, E.A. Payzant, J. Mater. Chem. 11 (2001) 3354.
[8] C. Lind, A.P. Wilkinson, C.J. Rawn, E.A. Payzant, J. Mater. Chem. 12 (2002) 990.
[9] C. Closmann, A.W. Sleight, J.C. Haygarth, J. Solid State Chem. 139 (1998) 424.
[10] U. Kameswari, A.W. Sleight, J.S.O. Evans, Int. J. Inorg. Mater. 2 (2000) 333.
[11] S. Zhang, X. Zhao, H. Ma, X. Wu, Chin. J. Chem. 18 (2000) 571.
[12] J.S.O. Evans, P.A. Hanson, R.M. Ibberson, N. Duan, U. Kameswari, A.W. Sleight, J. Am. Chem. Soc. 122 (2000) 8694.
[13] L. Huang, Q.G. Xiao, H. Ma, G.B. Li., F.H. Liao, Ch.M. Qi, X. Zhao, Eur. J. Inorg. Chem. 22 (2005) 4521.
[14] R. Zhao, X. Yang, H. Wang, J. Han, H. Ma, X. Zhao, J. Solid State Chem. 180 (2007) 3160.
[15] P.D. Pathak, N.G. Vasavada, Acta Crystallogr. A26 (1970) 655.
[16] C. Dong, J. Appl. Crystallogr. 32 (1999) 838.
[17] T.J.B. Holland, S.A.T. Redfern, Mineral. Mag. 61 (1997) 65.
[18] A.C. Larson, R.B. Von Dreele, General structure analysis system (GSAS), Los Alamos National Laboratory Report LAUR. 86, 2000.
[19] Q.G. Xiao, L. Huang, H. Ma, X. Zhao, J. Alloys Compd. 452 (2008) 446.
[20] X.B. Deng, J.Z. Tao, X. Yang, H. Ma, J.W. Richardson, X. Zhao, Chem. Mater. 20 (2008) 1733.